The smart Peano fluidic muscle: a low profile flexible orthosis actuator that feels pain

Allan Joshua Veale, Iain A. Anderson, Shane Q. Xie

Allan Joshua Veale, Iain A. Anderson, Shane Q. Xie, "The smart Peano fluidic muscle: a low profile flexible orthosis actuator that feels pain," Proc. SPIE 9435, Sensors and Smart Structures Technologies for Civil, Mechanical, and Aerospace Systems 2015, 94351V (27 March 2015); doi: 10.1117/12.2084130

SPIE.

Event: SPIE Smart Structures and Materials + Nondestructive Evaluation and Health Monitoring, 2015, San Diego, California, United States

The smart Peano fluidic muscle: a low profile flexible orthosis actuator that feels pain

Allan Joshua Veale[*a, b], Iain A. Anderson[b, c], Shane Q. Xie[a]
[a]Department of Mechanical Engineering, The University of Auckland, 20 Symonds Street, Auckland 1010, New Zealand; [b]Biomimetics Lab, Auckland Bioengineering Institute, 70 Symonds Street, Auckland 1010, New Zealand; [c]Department of Engineering Science, The University of Auckland, 70 Symonds Street, Auckland 1010, New Zealand

ABSTRACT

Robotic orthoses have the potential to provide effective rehabilitation while overcoming the availability and cost constraints of therapists. These orthoses must be characterized by the naturally safe, reliable, and controlled motion of a human therapist's muscles. Such characteristics are only possible in the natural kingdom through the pain sensing realized by the interaction of an intelligent nervous system and muscles' embedded sensing organs.

McKibben fluidic muscles or pneumatic muscle actuators (PMAs) are a popular orthosis actuator because of their inherent compliance, high force, and muscle-like load-displacement characteristics. However, the circular cross-section of PMA increases their profile. PMA are also notoriously unreliable and difficult to control, lacking the intelligent pain sensing systems of their biological muscle counterparts.

Here the Peano fluidic muscle, a new low profile yet high-force soft actuator is introduced. This muscle is smart, featuring bioinspired embedded pressure and soft capacitive strain sensors. Given this pressure and strain feedback, experimental validation shows that a lumped parameter model based on the muscle geometry and material parameters can be used to predict its force for quasistatic motion with an average error of 10 - 15N. Combining this with a force threshold pain sensing algorithm sets a precedent for flexible orthosis actuation that uses embedded sensors to prevent damage to the actuator and its environment.

Keywords: Peano, fluidic muscle, soft actuator, McKibben, artificial muscle, pain sensing, embedded sensing, orthosis

1. INTRODUCTION

People with physical disabilities such as stroke and spinal cord injuries have been treated with manual therapy for decades. However, the limited availability and high cost of skilled therapists[1] do not practically allow for the long, intense, frequent rehabilitation sessions required for effective rehabilitation[2-4]. In contrast, robots have been providing reliable and tireless labor on factory floors since the 1950s, and are now being adapted to emulate the task of a human therapist in the form of a wearable robotic orthosis, or exoskeleton. Robotic orthoses (hereon orthoses), are worn mechanically in parallel with the upper or lower limbs such that they work in tandem with the natural musculoskeletal system to assist the movement of those limbs. Importantly, they have been demonstrated to match the rehabilitative outcomes of manual therapy[5].

For orthoses to effectively deliver rehabilitative therapy, they must be characterized by the naturally safe, controlled, and fundamentally reliable motion of the muscles they are rehabilitating[6-8]. Biological muscles endure many actuation cycles in the uncertainty of the real world environment without sustaining damage due to their ability to intelligently sense and react to pain. Position and force detecting organs or 'sensors' are embedded within muscles that convey sensory data to the nervous system. Specifically, stretchable muscle spindles are located throughout skeletal muscle tissue to measure muscle position and motion. These, and the force sensing golgi tendon organs connecting muscle fibers and tendons, provide feedback for intelligent pain sensing[9]. Although the complex physiology of muscle spindles is not completely understood, research shows that pain receptors (nociceptors) in muscle spindles detect imminent and incurred muscle damage due to overexertion[10]. The nervous system interprets the signals from nociceptors as pain, to which one can

* Author to whom correspondence should be addressed: Allan Veale
Email: avea007@aucklanduni.ac.nz

Sensors and Smart Structures Technologies for Civil, Mechanical, and Aerospace Systems 2015, edited by Jerome P. Lynch, Kon-Well Wang, Hoon Sohn, Proc. of SPIE Vol. 9435, 94351V
 · doi: 10.1117/12.2084130

decide to act to mitigate muscle damage. Muscle spindles and possibly golgi tendon organs protect the muscle from temporary overloading through automatic regulation of muscle length and tension with the stretch and golgi tendon reflexes respectively[11, 12]. These reflexes act as a low-level control system that reacts independent of whether one consciously chooses to remove the loading condition threatening the muscle. Hence, embedded position and force sensing in biological muscles play a key role in the detection of pain and activation of reflex action that has the potential to mitigate muscle damage. These same attributes are desired in orthoses.

1.1 Fluidic muscles as orthosis actuators

Current orthoses are limited by their use of traditional electric, hydraulic, and pneumatic actuator technologies[6, 13-15]. Orthoses require actuators that are slim, powerful, and compliant to ensure an unobtrusive,[16, 17] efficient, and safe interaction with the wearer[18]. However, robotics' highly geared electric motors, hydraulic cylinders, and pneumatic actuators are bulky, heavy, and stiff for coupling to an orthosis and would compromise the limited space, wearability, and compliance required for safe interaction with changing, uncertain environments. In lieu of traditional actuators' unsuitability for slim and safe orthosis actuation, researchers have instead used fluidic muscles, and most popularly, the McKibben muscle, or pneumatic muscle actuator (PMA). A McKibben muscle is made of an elastomeric cylindrical bladder inside a braided tube of stiff flexible fibers. The braided tube and elastomeric cylinder assembly is terminated at its ends so that when filled with a fluid the pressure acting across its circumferential area causes the tubular structure to radially expand. The weave of the braided fibers serves to couple this radial expansion to longitudinal shortening of the muscle, generating a contractile force as the PMA shortens (Figure 1). Among the primary reasons cited for PMAs' popularity are their high specific force;[19] high specific power density (not accounting for the mass of their power source);[20, 21] inherent muscle-like compliance that can be varied through co-contraction of antagonistically arranged PMA pairs; flexibility; and remote placement from the prime mover[8]. Overall, the PMA is a powerful yet safe, soft actuator.

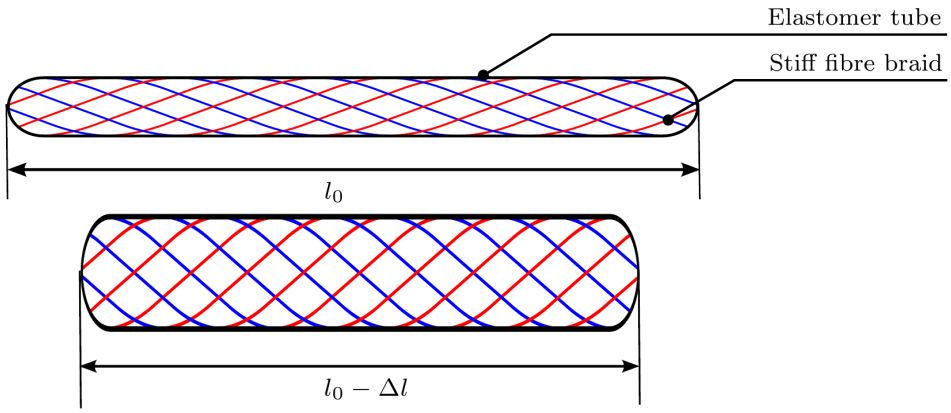

Figure 1. The McKibben fluidic muscle contracts from an initial length l_0 (top) by a displacement Δl when inflated with a fluid (bottom).

Although a promising fluidic muscle for orthosis actuation, PMA are not without their problems. The circular cross-section of PMA means that they have a minimum surface area, and therefore force generating capability for the volume that they occupy. This large dead volume slows their dynamic response, increases their bulk,[22, 23] and reduces their flexibility. PMA are also well known for their unreliability. This is due to their construction from soft, flexible materials that cannot be precisely characterized like the rigid materials of conventional electric, hydraulic, and pneumatic actuators[24]. For these same reasons PMA, and fluidic actuators in general, are difficult to control, preventing their effective use as an orthosis actuator[25, 26].

1.2 Embedded sensing in fluidic muscles

The pain sensing concepts used in biological muscles can be biomimetically transferred to detect and act on painful conditions for fluidic muscles such that they are not damaged by unexpected loads. However, the challenge is to do this without compromising the desired slim form factor and flexibility of the fluidic muscle. In the prior art a variety of novel embedded sensing techniques have been employed to measure fluidic muscle position and force. These can be summarized by their method of transduction, which rely on capacitive, resistive, piezoelectric, optical, or inductive

effects. Goulbourne *et al.* suggested dielectric elastomer based capacitive position sensing of PMA[27, 28]. However, the actual implementation of the sensor into a muscle was not clearly documented.

Among resistive PMA position sensors are Wakimoto *et al.*'s rubber sensor coated in conductive ink. It has a high sensitivity and is very flexible, but has a slow response and time dependent viscoelastic behavior[29]. Park and Wood embedded helical microchannels filled with a liquid conductor, eutectic Gallium Indium (eGaIn), into the walls of a Baldwin style PMA. This position sensing method showed a high linearity and low hysteresis. The addition of decoupled force sensing was also proposed by incorporating additional pressure sensitive eGaIn microchannels into the PMA wall[30]. Unfortunately, though promising, this method severely decreased PMA robustness.

Yamamoto *et al.* constructed a paste based piezoelectric polymer sensor mounted on a urethane rubber strip for position sensing of a soft PMA like actuator. However, it suffered from a large amount of hysteresis and some noise[31].

Akagi *et al.* used an optical method with internal photoreflectors to measure the inner diameter of a PMA and so estimate its length[32]. This sensing method was low cost, but reduced PMA flexibility.

Recently, the best example of truly integrated force and position sensing in a PMA is that of Felt and Remy's smart braid PMA. They calculated the force and position of a PMA to 0.5mm and 5N resolution respectively by measuring inductance and resistance changes of its insulated copper wire braid[33]. However, the use of copper wire as a muscle braid reduced its flexibility and made it more susceptible to bending fatigue. It was also not directly transferable to fluidic muscles with geometries significantly different to the McKibben muscle.

From the above literature, it can be seen that while some transduction methods have potential, there is not yet a definitive solution for the embedding of position and force sensing capabilities into fluidic muscles. Moreover, intelligent embedded sensing has not yet been used to bring about the much-needed enhancement of fluidic muscle reliability and control. It is hoped that the method outlined in the following sections of this paper will contribute to such a generic smart sensing solution for preventing damage to fluidic muscles as they naturally interact with their working environment. Section 2 outlines the concept of a slimmer alternative to the McKibben fluidic muscle; section 3 describes a possible solution to embedding the ability to sense displacement and force into this slimmer muscle; section 4 presents the results of testing this solution; and section 5 summarizes this paper's contributions.

2. PEANO FLUIDIC MUSCLE CONCEPT

Originally suggested as a linear pneumatic actuator by Sanan *et al.,*[34] the Peano[†] fluidic muscle (PFM) conceptually consists of a row of multiple sealed tubes fabricated from an inelastic impermeable material and connected along their length. Each tube is oriented so that its axial axis is perpendicular to the PFM's contractile force. Figure 2 shows how pressurizing the PFM with a fluid inflates the tubes from a flat to a circular cross-section such that the width of each tube decreases by distance Δl, causing the muscle to contract.

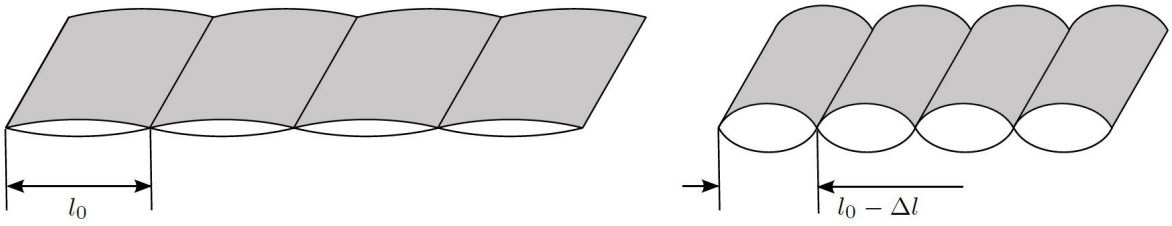

Figure 2. The tubes in a Peano fluidic muscle each contract from an initial width l_0 (left) by a displacement Δl when inflated with a fluid (right). This occurs as the tubes' cross-sectional area increases with inflation.

Like a PMA, the PFM has a limited muscle-like displacement with a force that decreases as it contracts. It also shares the compliance of the PMA through the compressibility of its working fluid and elasticity of its membrane. Additional compliance can be obtained by combining the concept of the McKibben braid with the PFM. Such a muscle would feature a composite membrane with a woven fiber in an elastic matrix. Orienting the fibers at an angle to the length axis of the fluidic muscle enable it to simultaneously use the Peano and McKibben effects to generate force.

[†] Referring to Giuseppe Peano, Italian mathematician and discoverer of the first space filling curve, as used to form the shape of the Peano fluidic muscle.

Both an ideal PFM and a PMA have a force generating capability proportional to the surface area of its membrane (the flexible surface on which fluid pressure acts). For a given muscle length, the force of a PMA can be increased by increasing its radius and hence dead volume and bulk. Increasing the force of a PFM is achieved by only increasing its width, such that its thickness is not affected. In practice, this means that a deflated PFM with the desired force can be made as slim as material strength and fabrication techniques allow. A further consideration to the PFM's slimness is the thickness and dynamic effects of the dead volume required to transfer fluid between muscle tubes. In contrast to PMA, the volume of PFM can be readily distributed over the surface of a human wearing a PFM actuated device, with the result of a slim yet high force fluidic muscle.

2.1 Quasistatic lumped parameter modeling of the Peano fluidic muscle

Modeling of the Peano fluidic muscle is in its infancy and has been limited to characterizing the relationship between its force, strain, and pressure for quasistatic motion (where hysteretic effects are ignored). Niiyama *et al.* proposed a virtual work method that enabled muscle force to be calculated from a parametric function involving muscle pressure, strain, and the included angle of the arc formed by each tube as it inflates. The muscle membrane tubes were assumed to have a constant width and zero bending stiffness. To account for the elasticity of the thermoplastic membranes used, a coefficient C_e was introduced and determined by fitting the model to raw force-strain data for a given pressure[35]. This empirically fitted model had the following limitations that the model presented here will attempt to address:

- Unpressurized membrane tensile properties were not directly used to predict muscle blocking force (the force generated when the muscle is fixed at its unstretched length and pressurized)
- Membrane tensile properties were not used to predict muscle behavior as it is stretched at zero pressure
- The tendency for the PFM's maximum contractile strain (free strain) to change as a function of pressure was not modeled
- The ideal muscle model was only solvable using numerical techniques
- The effect of a finite thickness flow passage interconnecting muscle tubes was unaccounted for

Here, the PFM is modeled by applying a force balance to a single muscle tube with the geometry shown in Figure 3. It is assumed that the properties of the N tubes that make up the PFM are sufficiently similar to be considered identical, and represented by those of the single tube. This tube has an unstretched membrane width w, a length l, a flow passage height h, and is filled with a pressure P to generate a contractile force F.

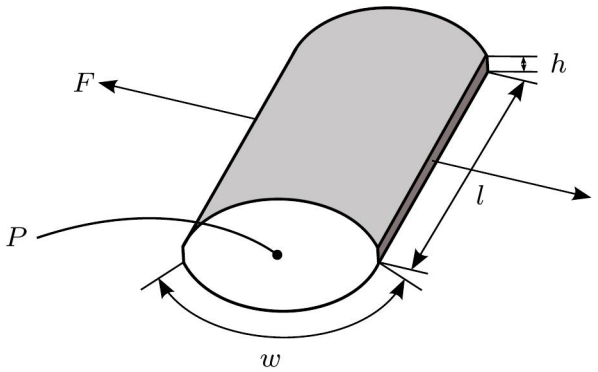

Figure 3. The geometry parameters of a single representative Peano fluidic muscle tube.

The behavior of the Peano tube is modeled by the four units shown on the left of Figure 4. The ideal contractile unit approximates the force generated by an ideal PFM. An ideal muscle with an infinitely stiff membrane generates an infinite force in its rest position that tends to zero as it reaches a contractile strain of $(\pi-2)/\pi \approx 0.36$. Here this behavior is approximated by a piston acting on a linkage with arms of length b. In the piston's rest position, with the linkage arms horizontal, it initially generates an infinite force against a load restraining the arms' motion. If b is sized

correctly with respect to *w,* then the linkage arms will reach their vertical, zero force position when they have traveled a horizontal displacement equivalent to the muscle tube contracting by a strain of 0.36. The piston is sized with a cross-sectional area *A1* that is the product of the muscle tube planform area *wl*; a factor of 0.8 that empirically recognizes that 20% of the muscle tube length does not generate force due to distortion of the muscle tube ends; and a factor of 0.74 that results in the optimal match between the approximation and parametric contractile models. Unlike Niiyama *et al.*'s ideal contractile model, the approximation can be solved explicitly and when the membrane stiffness is accounted for, the small error due to representing the tube as a piston driven linkage instead of an arc is insignificant.

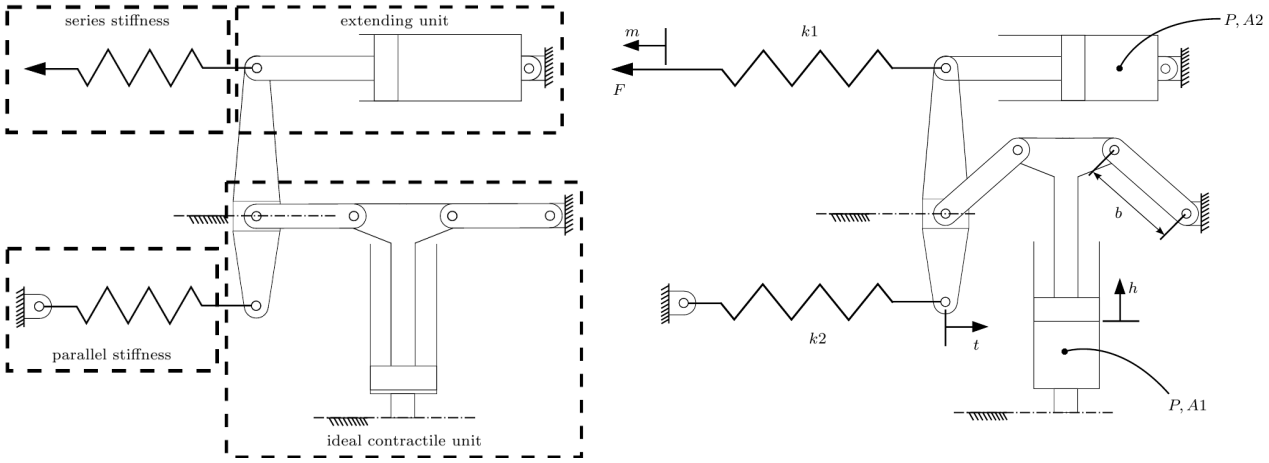

Figure 4. The quasistatic behavior of the PFM can be modeled as a force balance of four interacting units shown in their rest position (left) and in a partially actuated state (right).

The extending unit represents the force generated by fluid in the muscle tube acting across its flow passage cross-sectional area, *A2*. The series stiffness *k1* is the tensile stiffness of the muscle membrane as it is stretched unaxially in an unpressurized state. Lastly, a finite membrane bending stiffness *k2* is taken to act in parallel to the ideal contractile unit. This characterizes the tendency for the muscle tube free strain to be significantly lower than its theoretical maximum, and more so at lower pressures. In accordance with the mechanism in Figure 4, the geometry of the ideal contractile unit linkage produces a force F_{ideal}:

$$F_{ideal} = P \times A1 \frac{b - t/2}{\sqrt{b^2 - \left(b - t/2\right)^2}} \tag{1}$$

Recognizing the kinematic relation between muscle displacement *m,* and the ideal contractile unit displacement:

$$t = F/k1 - m \tag{2}$$

Applying the force balance equation to the four units gives:

$$F_{ideal} - F_{k2} - F_{extend} - F = 0 \tag{3}$$

Substituting in physical PFM parameters for the parallel stiffness force F_{k2}, the extending unit force F_{extend}, and equations (1) and (2) yields equation (4). This equation relates the PFM geometry and material parameters to its force, displacement, and pressure. With the aid of a numerical method, it can be used to predict PFM force as a function of the muscle pressure and strain.

$$P \times A1 \frac{b - \frac{1}{2}\left(F/_{k1} - m\right)}{\sqrt{b^2 - \left(b - \frac{1}{2}\left(F/_{k1} - m\right)\right)^2}} - k2\left(F/_{k1} - m\right) - P \times A2 - F = 0 \tag{4}$$

3. A SMART PEANO FLUIDIC MUSCLE

The smart Peano fluidic muscle is the practical realization of a fluidic muscle that uses the Peano force generation concept and embedded force and position feedback. The challenge in developing such an actuator is to simultaneously achieve the desired slim form factor, McKibben muscle-like force and displacement performance, and required feedback without compromising the flexibility of the fluidic muscle.

The smart PFM prototype presented in this paper (Figure 5) consists of a flexible membrane clamped at either end and constrained such that it forms four tubes when inflated. The prototype is slim with a total thickness, including its sensors, of 15mm. In contrast to previous embedded sensing of fluidic muscles, we have measured muscle displacement using StretchSense's soft capacitive strain sensor (StretchSense Ltd., Auckland, New Zealand) and muscle pressure with a MS5803-14BA digital interface micropressure transducer (Measurement Specialties, Fremont, CA). Given feedback from these sensors, equation (4) can then be used to estimate the muscle tensile force.

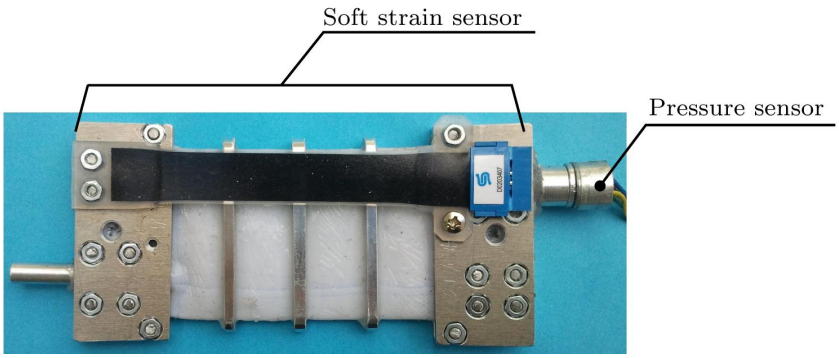

Figure 5. The smart Peano fluidic muscle has a capacitive strain sensor and a pressure sensor to aid force estimation

We have chosen to measure one state variable in the mechanical domain and one in the fluidic domain (rather than both in the mechanical domain) as this particular combination of sensor hardware enables the sensors to be integrated relatively easily into this, and other fluidic muscles, without significantly compromising the muscles' size, flexibility, or robustness. Pressure sensors are also significantly cheaper and smaller than load cells, and are usually required in the control of fluidic muscles; only here they are mounted directly to the muscle instead of the valve manifold. Capacitive strain sensors were chosen over variable resistance alternatives for their greater repeatability, accuracy, robustness, and off-the-shelf availability. This concept can also be extended to multi-degree-of-freedom fluidic actuators with the addition of enough soft strain sensors to determine the inflation state of the actuator.

4. TOWARDS PAIN SENSING PEANO FLUIDIC MUSCLES

The first step towards realizing pain sensing in the smart PFM is to validate the model of section 2.1 to verify that it can provide a reasonable estimate of muscle force using the bioinspired embedded sensing solution. Given that this solution is valid, we then need to determine how the muscle force and position feedback can be used to protect the muscle and the environment that it interacts with.

4.1 Quasistatic model validation

The prototype PFM shown in Figure 5 was used in all the validation experiments of the lumped parameter force model. It is characterized by the geometry and material parameters in Table 1. The tensile stiffness $k1$ was determined from fitting a stiffness function to raw data obtained by stretching the unpressurized PFM uniaxially. With respect to Figure 4 this stiffness acts on the displacement $m + t$, which is combined with equation (2) to get the relation in the table below.

Table 1. The geometry and material parameters that characterize the smart Peano fluidic muscle prototype. Note that units are in meters, meters squared, and Newtons per meter for distance, area, and stiffness respectively.

Geometry parameters	Material parameters
$w = 0.01725$	$k1 = 26.99 \times 10^3 + \sqrt{728.2 \times 10^6 + 191.8 \times 10^6 F}$
$l = 0.046$	
$h = 0.002$	
$b = w(\pi - 2)/(2\pi)$	
$A1 = 0.74(w \times 0.8l)$	$k2 = 1.2 \times 10^{15} t^4$
$A2 = hl$	

The bending stiffness of the membrane, *k2*, was determined by substituting experimentally obtained free strain values into equation (4) with a force of zero; solving for *k2* at various muscle displacements; and fitting a curve to *k2* as a function of *t*. Due to the difficulty of resolving free strain values at zero force, the free strain values were taken at a force value of 10N.

The PFM prototype was placed in a tensile testing device and its force and contractile strain measured during quasistatic unloading - loading experiments at four pressures. Each experiment was repeated three times, and the results, along with the model described by the parameters of Table 1, are in Figure 6. Given that the model does not account for the PFM's hysteresis, it predicts the experimental data reasonably well across all tested pressures up to a contractile strain of about 0.1. At higher strains, the PFM force is underestimated and at moderate strains it is slightly overestimated. The model also consistently underestimates the PFM blocking force and does not capture the non-zero force for positive contractile strains at a pressure of 0kPa. The last two observations can be accounted for by the model's exclusion (for simplicity) of an additional stiffness element representing the soft strain sensor. The presence of this sensor introduces an additional small tensile force acting in parallel with the whole muscle. The reduced accuracy of the model at higher strains is not a significant issue in practical applications because the PFM would normally be designed to operate outside of this region due to its low force generating capability at strains close to its free strain. However, model accuracy in this regard could be improved by gaining a better understanding of how membrane bending stiffness varies as the muscle approaches the free strain condition. In particular, the model needs to capture the rapid increase in *k2* as the seams connecting adjacent muscle tubes stiffens at large strains. This would also require a more precise load cell.

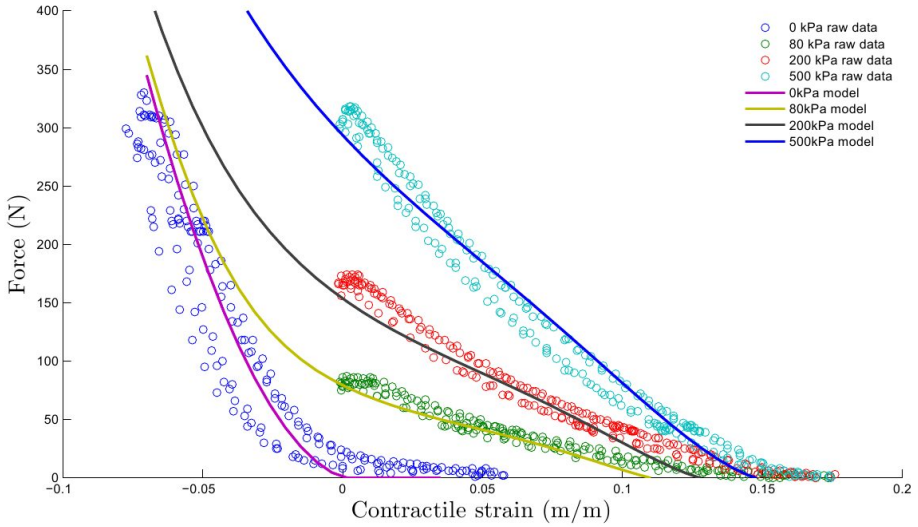

Figure 6. The experimental and model predicted force-strain characteristics of the prototype Peano fluidic muscle.

After comparing the PFM modeled and experimental characteristics, data was recorded from the embedded sensors on the PFM as it was manually loaded and unloaded in an arbitrary manner. PFM pressure was simultaneously ramped from 0-500kPa and back to 0kPa. The lumped parameter model was then used to estimate the muscle force for comparison with the muscle force recorded by the tensile testing device. Figure 7 (top-left) shows that the embedded pressure sensor

accurately measured the test pressure applied to the PFM. The strain sensor provided a strain measurement (green trace, top-right) that closely followed the trend of the actual PFM strain (blue trace, top-right). The small strain error between the two measurements, most significant at higher strain rates, appears to be due to the level of averaging applied to cancel noise in the capacitance data. Provided the strain sensor is suitably isolated from noise, decreasing the number of samples over which the averaging filter in the strain sensor hardware acts would allow the embedded sensor and test device strain readings to match at higher strain rates with even more accuracy. Using the strain data with an average error of 0.005m/m, a force estimate with an average error of 10 - 15N, and a maximum of about 25N was obtained. The force estimate data (green trace, bottom-left) for the pressure and strain measurements shown roughly matched the trend and magnitude of the actual force (blue trace, bottom-left). Surprisingly, it corresponded better to the actual force than a force estimate made using the test device pressure and strain readings. This suggests that the soft strain sensor readings better represented the PFM length than the strain measurements taken by the test device. A reasonable explanation is the ability of the strain sensor to move with the muscle as it twists upon inflation (due to slight unevenness in muscle tube widths) whereas the test rig only measures movement between the pivoted muscle center mounts without accounting for the twisting effect. Force estimation of a constant 100N force (bottom-right) as the PFM pressure and strain varied simultaneously (to a peak of 500kPa and 0.08 respectively) revealed a slowly fluctuating force estimate. Notably, the estimate was above the true force. This is thought to be a combined effect of the model's overestimation of force data for moderate contractile strains (an effect that increases with pressure as in Figure 6) and strain measurement errors caused by overaveraging of the strain sensor data. It is also possible that the strain sensor caught on the metal bands constraining the muscle tubes, creating jerks in the strain measurement. This could be resolved by securing the strain sensor to each of the muscle tube bands.

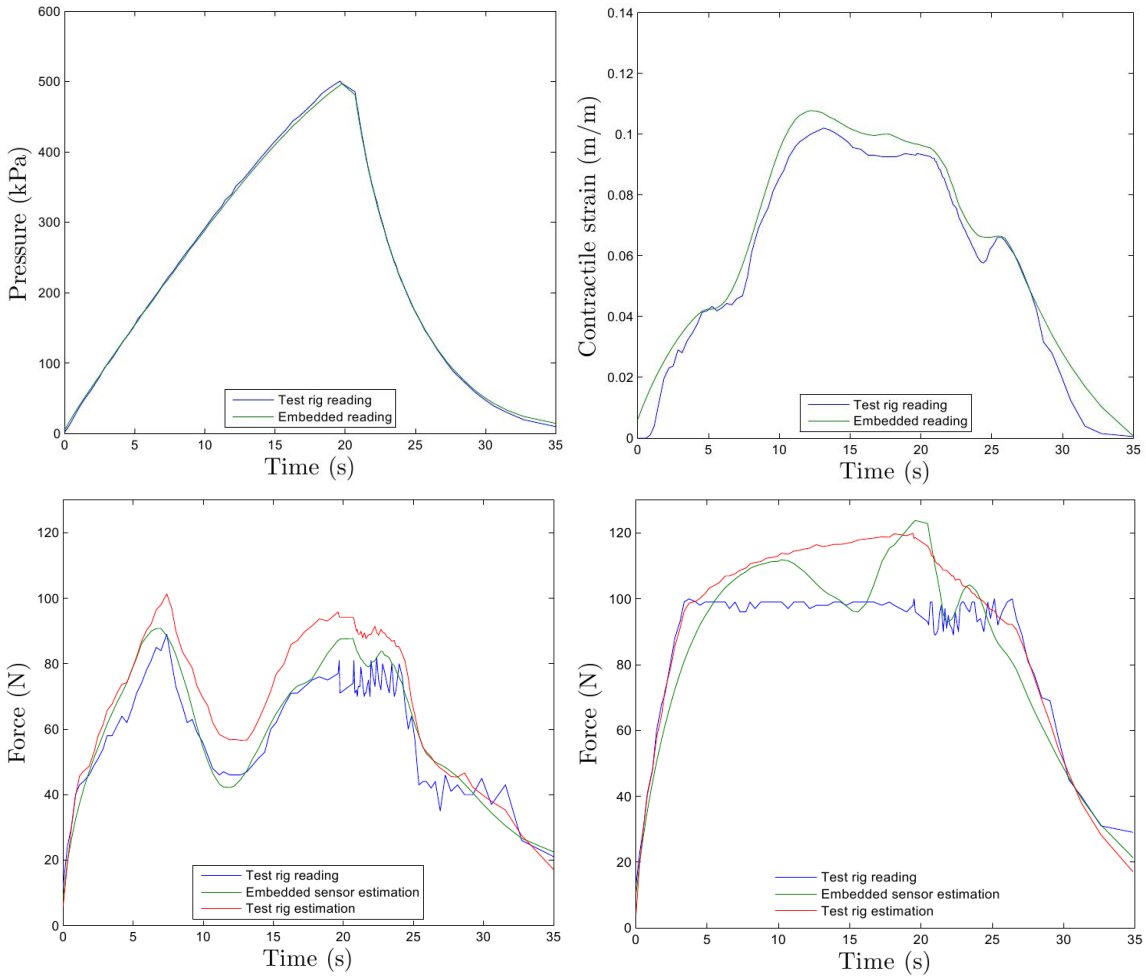

Figure 7. The pressure (top-left) and strain (top-right) measurements with corresponding force estimation (bottom-left) for the smart Peano fluidic muscle. Force estimation using embedded sensing for a constant force level (bottom-right).

4.2 Detection of fluidic muscle pain

Recognizing the limitations of the PFM model, a simple way of detecting pain is to use a force threshold. If the force estimate calculated from the embedded sensors and lumped parameter model is above the threshold value, action needs to be taken to prevent damage from occurring, as in biological systems. An example of how this would work is illustrated by Figure 8. Here, the calculated force estimate is compared to a threshold of 50N. It is supposed that above this threshold damage would be done to the muscle. The green region indicates combinations of sensor readings that correspond to an allowable estimated force, the red region a force greater than 50N, and the yellow region sensor reading combinations not valid for the given muscle geometry. More sophisticated approaches would account for uncertainty in the model and sensor readings; the fluidic muscle dynamics; a pain level depending on how high the force is above the threshold; and accumulated pain over time to arrive at a muscle 'health'. All of these advances in smart embedded sensing would move fluidic muscle technology closer to realizing improved robustness and safety.

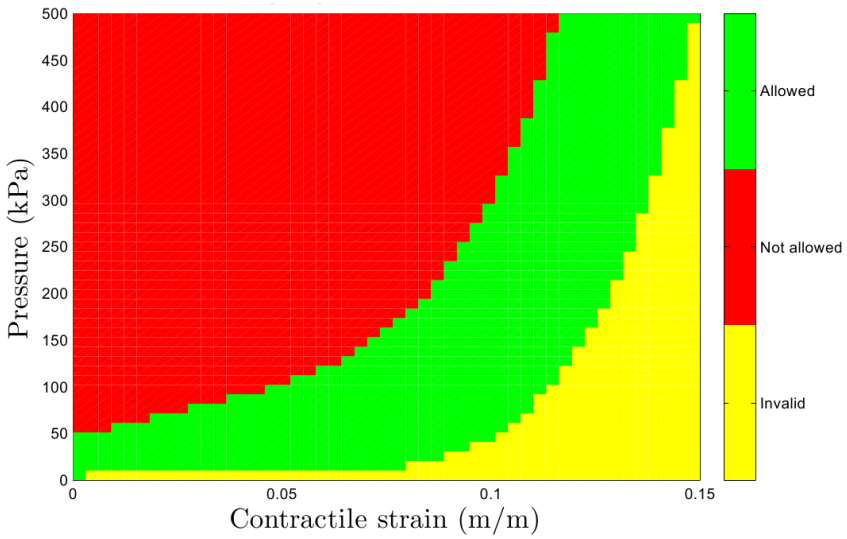

Figure 8. The predicted allowable operating region for the prototype Peano fluidic muscle with a force threshold of 50N.

5. CONCLUSIONS

This paper presents the concept, fabrication, and lumped parameter modeling of the Peano fluidic muscle, a low-profile alternative to the McKibben muscle particularly suitable for discreet orthosis actuation. The robustness and safety of these and other fluidic muscles can be improved through the use of embedded soft capacitive strain sensors, micropressure transducers, models that estimate muscle force as a function of its pressure and strain state, and bioinspired pain sensing algorithms. Here, the Peano fluidic muscle model was based on the muscle geometry and membrane tensile and bending stiffnesses. It was used with a smart Peano fluidic muscle to obtain a force estimate with an average error of 10 - 15N and a maximum error of about 25N. An example was given of how even a simple force threshold can be used to indicate and mitigate damage to the muscle and its environment.

In future work the accuracy of the model can be improved by enhancing it to capture hysteresis, more realistic membrane bending stiffness, and force generation at high strains. Finally, steps need to be taken to develop more sophisticated pain sensing algorithms that account for real world uncertainties and accumulation of damage over time.

6. ACKNOWLEDGEMENTS

The authors acknowledge the financial support of The University of Auckland Doctoral Scholarship, and engineering expertise and equipment of Dean Veale of Alloy Blocks Ltd.

REFERENCES

[1] Keller, T. and Veneman, J., "Robotics for neurorehabilitation: Current state and future challenges," Applied Mechanics and Materials, 245, 3-8 (2013).

[2] Bütefisch, C., Hummelsheim, H., Denzler, P. and Mauritz, K., "Repetitive training of isolated movements improves the outcome of motor rehabilitation of the centrally paretic hand," J. Neurol. Sci., 130(1), 59-68 (1995).

[3] Kwakkel, G., Kollen, B. J. and Krebs, H. I., "Effects of robot-assisted therapy on upper limb recovery after stroke: A systematic review," Neurorehabil. Neural Repair, 22(2), 111-121 (2008).

[4] Bayona, N. A., Bitensky, J., Salter, K. and Teasell, R., "The role of task-specific training in rehabilitation therapies," Top. Stroke Rehabil., 12(3), 58-65 (2005).

[5] Klamroth-Marganska, V., Blanco, J., Campen, K., Curt, A., Dietz, V., Ettlin, T., Felder, M., Fellinghauer, B., Guidali, M., Kollmar, A., Luft, A., Nef, T., Schuster-Amft, C., Stahel, W. and Riener, R., "Three-dimensional, task-specific robot therapy of the arm after stroke: A multicentre, parallel-group randomised trial," Lancet Neurol., 13(2), 159-166 (2014).

[6] Mohammed, S., Amirat, Y. and Rifai, H., "Lower-limb movement assistance through wearable robots: State of the art and challenges," Adv. Rob., 26(1-2), 1-22 (2012).

[7] Wolff, J., Parker, C., Borisoff, J., Mortenson, W. B. and Mattie, J., "A survey of stakeholder perspectives on exoskeleton technology," J. Neuroeng. Rehabil., 11(169), 1-17 (2014).

[8] Caldwell, D. G., Tsagarakis, N. G., Kousidou, S., Costa, N. and Sarakoglou, I., "'Soft' exoskeletons for upper and lower body rehabilitation - design, control and testing," Int. J. Hum. Robot., 4(3), 549-573 (2007).

[9] Mileusnic, M. P. and Loeb, G. E., "Force estimation from ensembles of Golgi tendon organs," J. Neural Eng., 6(3), 1-15 (2009).

[10] Lund, J. P., Sadeghi, S., Athanassiadis, T., Salas, N. C., Auclair, F., Thivierge, B., Arsenault, I., Rompré, P., Westberg, K. G. and Kolta, A., "Assessment of the potential role of muscle spindle mechanoreceptor afferents in chronic muscle pain in the rat masseter muscle," PLoS ONE, 5(6), 1-21 (2010).

[11] Wang, Z., Li, L. Y. and Frank, E., "The role of muscle spindles in the development of the monosynaptic stretch reflex," J. Neurophysiol., 108(1), 83-90 (2012).

[12] Chalmers, G., "Strength training: Do Golgi tendon organs really inhibit muscle activity at high force levels to save muscles from injury, and adapt with strength training?" Sports Biomechanics, 1(2), 239-249 (2002).

[13] Dollar, A. M. and Herr, H., "Lower extremity exoskeletons and active orthoses: Challenges and state-of-the-art," IEEE Trans. Robot., 24(1), 144-158 (2008).

[14] Lo, H. S. and Xie, S. Q., "Exoskeleton robots for upper-limb rehabilitation: State of the art and future prospects," Med. Eng. Phys., 34(3), 261-268 (2012).

[15] Huo, W., Mohammed, S., Moreno, J. C. and Amirat, Y., "Lower limb wearable robots for assistance and rehabilitation: A state of the art," IEEE Syst. J. (to be published).

[16] Kleinjan, J. G., Dunning, A. G. and Herder, J. L., "Design of a compact actuated compliant elbow joint," Int. J. Struct. Stab. Dyn. (2014).

[17] Rocon, E., Belda-Lois, J. M., Ruiz, A. F., Manto, M., Moreno, J. C. and Pons, J. L., "Design and validation of a rehabilitation robotic exoskeleton for tremor assessment and suppression," IEEE Trans. Neural Syst. Rehabil. Eng., 15(3), 367-378 (2007).

[18] Hollander, K. W., Sugar, T. G. and Herring, D. E., "Adjustable robotic tendon using a 'jack spring'™," Proc. 2005 IEEE 9th Int. Conf. Rehabilitation Robotics, 113-118 (2005).

[19] Mori, M., Suzumori, K., Takahashi, M. and Hosoya, T., "Very high force hydraulic McKibben artificial muscle with a p-phenylene-2,6-benzobisoxazole cord sleeve," Adv. Rob., 24(1-2), 233-254 (2010).

[20] Hannaford, B. and Winters, J. M., [Actuator Properties and Movement Control: Biological and Technological Models], Springer-Verlag, New York, NY, 101-120 (1990).

[21] Chou, C. and Hannaford, B., "Measurement and modeling of McKibben pneumatic artificial muscles," IEEE Trans. Robot. Autom., 12(1), 90-102 (1996).

[22] Davis, S., Canderle, J., Artrit, P., Tsagarakis, N. and Caldwell, D. G., "Enhanced dynamic performance in pneumatic muscle actuators," IEEE Int. Conf. Robot. Autom., 2836-2841 (2002).

[23] Park, Y., Santos, J., Galloway, K. G., Goldfield, E. C. and Wood, R. J., "A soft wearable robotic device for active knee motions using flat pneumatic artificial muscles," IEEE Int. Conf. Robot. Autom., 4805-4810 (2014).

[24] Kingsley, D. A. and Quinn, R. D., "Fatigue life and frequency response of braided pneumatic actuators," Proc. 2002 IEEE Int. Conf. Robot. Autom., 830-832 (2002).

[25] Vo-Minh, T., Tjahjowidodo, T., Ramon, H. and Van Brussel, H., "A new approach to modeling hysteresis in a pneumatic artificial muscle using the Maxwell-slip model," IEEE Trans. Mechatron., 16(1), 177-186 (2011).

[26] Wolbrecht, E. T., Leavitt, J., Reinkensmeyer, D. J. and Bobrow, J. E., "Control of a pneumatic orthosis for upper extremity stroke rehabilitation," Proc. 28th IEEE EMBS Annu. Int. Conf., 2687-2693 (2006).

[27] Goulbourne, N. C. and Son, S., "Numerical and experimental analysis of McKibben actuators and dielectric elastomer sensors," ASME Int. Mech. Eng. Congr. Expo., 175-186 (2007).

[28] Goulbourne, D. N. C., Son, S. and Fox, J. W., "Self-sensing McKibben actuators using dielectric elastomer sensors," Electroactive Polymer Actuators and Devices (EAPAD) 2007, 1-12 (2007).

[29] Wakimoto, S., Suzumori, K. and Kanda, T., "Development of intelligent McKibben actuator with built-in soft conductive rubber sensor," 13th Int. Conf. Solid-State Sensors Actuators Microsystems, TRANSDUCERS '05, 745-748 (2005).

[30] Park, Y. L. and Wood, R. J., "Smart pneumatic artificial muscle actuator with embedded microfluidic sensing," 12th IEEE Sensors Conf., 1-4 (2013).

[31] Yamamoto, Y., Kure, K., Iwa, T., Kanda, T. and Suzumoru, K., "Flexible displacement sensor using piezoelectric polymer for intelligent FMA," 2007 IEEE/RSJ Int. Conf. Intell. Robots Syst., 765-770 (2007).

[32] Akagi, T., Dohta, S., Kenmotsu, Y., Zhao, F. and Yoneda, M., "Development of smart inner diameter sensor for position control of Mckibben artificial muscle," 2nd Int. Symp. Robot. Intell. Sensors 2012, 105-112 (2012).

[33] Felt, W. and Remy, C. D., "Smart braid: Air muscles that measure force and displacement," 2014 IEEE/RSJ Int. Conf. Intell. Robots Syst., 2821-2826 (2014).

[34] Sanan, S., Lynn, P. S. and Griffith, S. T., "Pneumatic Torsional Actuators for Inflatable Robots," J. Mechanisms Robotics, 6(3), 1-7 (2014).

[35] Niiyama, R., Rus, D. and Kim, S., "Pouch motors: Printable/inflatable soft actuators for robotics," IEEE Int. Conf. Robot. Autom., 6332-6337 (2014).